Catalytic and Inhibitory Effects Induced by Noncovalent Interactions between Cellulose and

Lignin During Fast Pyrolysis

Fuat Sakirler, M. Doga Tekbas, and Hsi-Wu Wong*

Department of Chemical Engineering, University of Massachusetts Lowell

One University Avenue, Lowell, Massachusetts 01854, United States

Corresponding Author

*E-mail: hsiwu wong@uml.edu

Abstract

Biomass fast pyrolysis has emerged as a highly promising technology for producing renewable

fuels and chemicals. However, the inherent multi-scale and multiphase nature of the process and

the heterogeneous nature of biomass feedstocks typically lead to low selectivity toward each bio-

oil molecule, posing significant commercialization challenges. Molecular-level understanding of

the biomass pyrolysis reaction kinetics considering the interactions between the main constituents

(i.e., cellulose, hemicellulose, and lignin) is essential to advance the macroscopic design, scale-up,

and optimization of the process. In this work, microreactor experiments were conducted to

determine the effects of lignin structures on the yields of cellulose-derived products during

pyrolysis. We show that levoglucosan formation is inhibited by the β-O-4 lignin linkages or

catalyzed by the 5-5 linkages, glycolaldehyde formation is catalyzed by the β-O-4 linkages or

inhibited by the 5-5 linkages, and 5-hydroxymethylfurfural formation is inhibited by either linkage.

Density functional theory calculations reveal that these catalytic and inhibitory effects on cellulose

fast pyrolysis are induced by noncovalent interactions between cellulose and lignin. The molecular-

level picture of cellulose–lignin interactions uncovered in this work paves the way for further use

of genetic engineering to grow new genotypes of biomass for selective production of value-added chemicals and machine learning approaches to obtain correlations between biomass structures and product yields for biomass fast pyrolysis.

Keywords:

Biomass fast pyrolysis; cellulose–lignin interactions; density functional theory; noncovalent interactions; reaction kinetics

Introduction

Bioenergy is the most predominant contributor to renewable energy, accounting for approximately 55% of global renewable energy use and more than 6% of global energy supply in 2021.¹ Among various biomass conversion methods, fast pyrolysis, which is thermal decomposition in the absence of oxygen, offers an inexpensive and simple route toward producing renewable fuels and chemicals.² Fast pyrolysis of lignocellulosic (inedible) biomass can lead to liquid (i.e., bio-oil) yields as high as 75 wt% under typical operation conditions (e.g., temperature of 400–600°C and residence time of less than 10 s).³ However, the inherent multi-scale and multiphase nature of the pyrolysis process and the heterogeneous nature of biomass feedstocks typically lead to diverse product distributions where low selectivity toward each bio-oil molecule is commonly observed, presenting significant challenges in its commercialization.²⁻⁴

Three main biomass constituents exist: cellulose (CE, 30–55 dry wt%), hemicellulose (13–35 dry wt%), and lignin (14–36 dry wt%). Trace amounts of extractives (e.g., tannins, fatty acids, and resins) and alkaline earth salts (e.g., potassium, sodium, etc.) are also present. CE is a linear homopolymer of D-glucose connected with β-1,4-glycosidic linkages, decomposing at 315–400°C due to its highly crystalline structure held by hydrogen bonds and van der Waals forces. Hemicellulose is an amorphous polymer of various monosaccharides such as D-xylose, D-glucose, and D-mannose. It is the least thermally stable, decomposing at 220–315°C. Lignin decomposes at a wider temperature range of 160–900°C. It has an amorphous, cross-linked structure produced by the polymerization of three major monolignols (viz., p-coumaryl alcohol (H), coniferyl alcohol (G), and sinapyl alcohol (S)) in the plant cells, which are connected by various types of C–O and C–C linkages. The abundance of these monolignols as well as linkages significantly varies dependent on the plant types and the pretreatment methods used.

The interactions between the three biomass constituents are inherently intricate in the plant cell wall, involving covalent bonds and noncovalent interactions (NCIs) such as hydrogen bonds, π - π stacking, and van der Waals forces. 5 When operating in concert, such NCIs can result in differences in Gibbs free energy, leading to transition-state stabilization or destabilization. 12,13 Understanding the effects of these interactions at the molecular level is essential to the macroscopic process design, scale-up, and optimization of biomass fast pyrolysis technologies to obtain the most desirable product distributions.^{2,14} In particular, the interactions between CE and lignin during fast pyrolysis has been a subject of extensive research over the last two decades, yet no conclusive consensus has been reached. 15-17 Early experimental studies postulated that CE-lignin interactions affect secondary decomposition of levoglucosan (LG, 1,6-anhydro-β-D-glucopyranose). However, contradictory findings in LG yields lead to different hypotheses regarding the effects of lignin in the literature, 18-21 where inhibited LG polymerization, inhibited LG degradation, or catalyzed LG degradation is proposed. These differences may be attributed to the variability of lignin structures derived from various feedstocks, where different CE-lignin interactions and resulting pyrolysis pathways are present.^{6,21} Elucidating how these interactions alter CE pyrolysis pathways in the condensed phase requires the use of isotopic labelling or quantum chemistry calculations.²² The latter is known to be an inexpensive means to obtain insights into the reaction mechanism and kinetics of biomass pyrolysis. Our recent study on co-pyrolysis between CE and thermoplastics suggests that the formation of CE-derived products such as LG, glycolaldehyde (GA), and 5hydroxymethylfurfural (5-HMF) is catalyzed or inhibited by NCIs induced by functional groups in molten thermoplastics.²³ These NCIs between CE and thermoplastics altered formation kinetics of CE-derived volatiles and thus their yields. Similar NCIs could also be present between CE and lignin, potentially affecting reaction kinetics of biomass fast pyrolysis.

In this study, a combined experimental and quantum chemistry approach is used to elucidate the effects of the NCIs between CE and lignin on CE fast pyrolysis. A microreactor was designed to perform pyrolysis experiments under vacuum, reducing vapor residence time and precluding secondary degradation reactions in the gas phase. Co-pyrolysis experiments of CE with two different lignin dimers, namely guaiacylglycerol-β-guaiacyl ether (a G-β-O-4-G model compound) and 2,2'-dihydroxybiphenyl (a H-5-5-H model compound), were conducted, allowing studying the effect of different lignin linkage motifs. Density functional theory (DFT) calculations were also performed to investigate the formation pathways of key CE-derived products using cellobiose as a model compound. The DFT-calculated rate parameters of cellobiose decomposition into LG, GA, and 5-HMF in the presence of lignin dimers were compared to the experimental selectivity toward these products. This work demonstrates how lignin linkage motifs can modulate the kinetics of critical reaction pathways of CE fast pyrolysis by inducing NCIs, leading to catalytic (accelerated) or inhibitory (decelerated) effects.

Methods

Materials. Microcrystalline CE (degree of polymerization = 219, bulk density = 0.28 g mL⁻¹) was purchased from Alfa Aesar. G-β-O-4-G (97+%, $M_w = 320.34$ g mol⁻¹) was purchased from TCI. H-5-5-H (99%, $M_w = 186.21$ g mol⁻¹, density = 1.34 g mL⁻¹) and octacosane (C28, 99+%, $M_w = 394.77$ g mol⁻¹, density = 0.8067 g mL⁻¹) were purchased from Thermo Scientific Chemicals.

Sample preparation. CE thin-film samples with a thickness of 111.84 μm were prepared in copper sample holders according to the thin-film deposition method used in Paulsen *et al.*²⁴ The thickness of the binary samples containing CE and one of C28, G- β -O-4-G, and H-5-5-H was kept constant at 223.68 μm by changing mass loadings according to their individual density. The mass loadings of CE, C28, G- β -O-4-G, and H-5-5-H in the neat and co-pyrolysis experiments were 5.00, 2.60,

4.05, and 4.25 mg, respectively. These binary samples were mixed homogeneously and melted at 120° C according to the method described in our previous work.²³ In addition to the co-pyrolysis experiments, neat pyrolysis of C28, G- β -O-4-G, and H-5-5-H without CE was performed as controls following the same procedure (with a thickness of $111.84 \, \mu m$).

Pyrolysis experiments. The pyrolysis and co-pyrolysis experiments were performed with a custom-made batch reactor (Figure S1 of the Supporting Information) with a reaction time of 15 min according to the method used in our previous work.²³ The temperature of the reactor was controlled with a proportional-integral-derivative controller (Omega Engineering, CN742). Our reactor was designed to carry out pyrolysis experiments under vacuum (<0.04 torr) in a closed system where rapid heating of the samples was achieved via heat conduction. The reaction zone was preheated to the target reaction temperature (500°C) before a copper sample holder was swiftly dropped into the preheated reactor zone (500°C) by gravity from its initial position kept at room temperature. Based on the heat transfer model presented in our previous work, the initial heating rate of the samples in our experiments could reach as high as 2,300°C s⁻¹.²³ This enabled us to study the reaction kinetics of cellulose pyrolysis without heat transfer effects. Although our sample thickness was larger, the LG yield (15.9 percent carbon) from our previous neat CE pyrolysis experiment²³ at 500°C was found to be comparable to those (11–20 percent carbon) from the thinfilm pyrolysis of samples of 10-50 µm in a Frontier micropyrolyzer, 25 where chemical kinetics was determined to be limiting.²⁴ All the volatile products were collected in a condenser immersed in a liquid N₂ bath. The wall effects in our experiments were minimized by continuously removing the volatile products via rapid thermal diffusion (mimicking semi-batch operations) into the condenser and heating the reactor tube prior to dropping the copper sample holder. After each reaction, the condenser tube was quickly removed from the liquid N₂ bath, and the volatile products within, along with those in the transfer line, were immediately extracted by equal volume of methanol and dichloromethane. Each experiment was repeated three times in this work for reproducibility. The standard deviations of the three runs are reported as error bars in the figures.

Analytical methods. The reaction products were analyzed by gas chromatography (GC) according to the method reported in our previous work.²³ Briefly, gaseous and liquid products were analyzed using a Shimadzu GC-2010 Plus GC system equipped with a mass spectrometer and a flame ionization detector (FID) and a Shimadzu GC-2014 system equipped with a thermal conductivity detector and a FID. The mass of the produced char was calculated by the difference in weight of the copper sample holder before and after the reaction measured by a Mettler Toledo XP105 analytical balance. Note that it was impractical to carry out condenser tube weighing at the end of each experiment to measure the total mass of the volatile products due to the risk of losing the products from evaporation. In addition, significant moisture condensation outside the condenser tube wall was present due to low wall temperature caused by the liquid N₂ bath, preventing us from accurate mass measurement. As a result, we opted for immediate extraction of the volatile products in the condenser tube after each reaction, enabling the identification and accurate quantification of these products *via* GC.

Computational Methods. DFT calculations were performed according to the method used in our previous work.²³ Briefly, theoretical kinetics and thermodynamics calculations were conducted in the gas phase based on the M06-2X functional,²⁶ 6-31+G(2df,p) basis set, and D3 London-dispersion correction²⁷ using the Gaussian 16 package.²⁸ Atomic charges were calculated with the CHelpG scheme.²⁹ The quasi-rigid-rotor-harmonic-oscillator approach³⁰ with cut-off frequency of 150 cm⁻¹ was employed to treat low-frequency vibrational modes. In our DFT calculations, cellobiose and cellubiosan, dimers of CE containing a β-1,4 glycosidic bond, were used as

surrogates to study the pyrolysis pathways of CE and active CE, respectively. Propane (C3) was used as a surrogate for C28. Lignin model compounds include H, G, and S monomer units as well as dimers connected with various linkages, including G-β-O-4-G, 1-(4-Hydroxyphenyl)-2-(2methoxyphenoxy)propane-1,3-diol 1-(4-hydroxy-3-methoxyphenyl)-2- $(H-\beta-O-4-G)$, phenoxypropane-1,3-diol (G-β-O-4-H), 4-(1,3-Dihydroxy-2-phenoxypropyl)phenol (H-β-O-4-H), 3,3'-dimethoxy(1,1'-biphenyl)-2,2'-diol (G-5-5-G), H-5-5-H, and 4-(3-hydroxymethyl-5-(3hydroxyprop-1-enyl)-7-methoxy-2,3-dihydro-1-benzofuran-2-yl)-2-methoxyphenol While using dimers as model compounds clearly has limitations in modeling possible effects involving neighboring monomer units or linkages, particularly solvation effects where the impact of chain length could be critical, they allow more accurate determination of the reaction kinetics only involving in the linkages or motifs of interest as parts of the reaction center. Since the focus of this work is to establish detailed mechanistic understanding of the NCIs between key cellulose and lignin motifs, the dimer surrogates with both appropriate linkage structures and proper substitution patterns were selected. Based on the recommendation of Lahive et al.,⁶ this level of complexity (i.e., the "Level 2" complexity) is sufficient to provide insight into the reactivity of the specific motifs and types of products expected.

Results and discussion

Selection of the lignin surrogates. An initial screening using DFT was first carried out to understand how different lignin monolignols and linkages affect CE fast pyrolysis. This screening focused on the concerted cleavage of the glycosidic C–O bonds along CE chains, a key reaction in CE pyrolysis leading to LG formation.³¹ Given the complexity (**Figure S3**) and variability of lignin structures (**Table 1**), the choice of lignin surrogates presents a tradeoff between accurate representation of complex lignin structures and computational cost.⁶ Comparison of relative rate

constants without any external molecules (i.e., neat) against those in the presence of lignin surrogates serves as an indicator of catalytic ($k_{\text{lignin}}/k_{\text{neat}}>1$) or inhibitory ($k_{\text{lignin}}/k_{\text{neat}}<1$) effect induced by the lignin surrogates.²³

Table 1. Abundance of lignin monolignols and common linkages connecting the aromatic C₉ units in different feedstocks⁶⁻¹¹

	Monolignols (%)			Linkages ^{a,b} (%)					
Lignin	Н	G	S	β-Ο-4	4-O-5	5-5	β-5	β-β	β-1
Softwood	5–22	78–95	~0	45–65	0–7	5–27	6–12	2–6	1–9
Hardwood									
Grasses	5–37	26–80	14–55	74–84	nd	~1	5–14	1–7	~1

^a Abundance per 100 C₉ units

Figure 1 shows the ratio of rate constants at 500°C for C–O bond cleavage of cellobiosan in the presence of monomeric and dimeric lignin surrogates (corresponding to the kinetic parameters listed in **Table S2** and the structures of lignin surrogates shown in **Figure S3**). Based on the DFT results, the presence of a H unit induces a catalytic effect on C–O bond cleavage, whereas the presence of a G or S unit leads to an inhibitory effect. The catalytic effect induced by the H unit can be attributed to the hydroxyl group at the 4-position, where transition-state stabilization takes place through the creation of hydrogen bonds with lignin hydroxyls.^{25,32-35} On the other hand, our recent study suggests that transition states (TSs) of glycosidic bond cleavage of CE could be destabilized *via* the steric interactions invoked by the ether groups of polyethylene glycol during

b nd = not determined

its co-pyrolysis with CE.²³ In line with this steric phenomenon, the inhibitory effect induced by the G or S unit can be attributed to the methoxy group(s) at the 3- and 5-positions (**Figure S3a**).

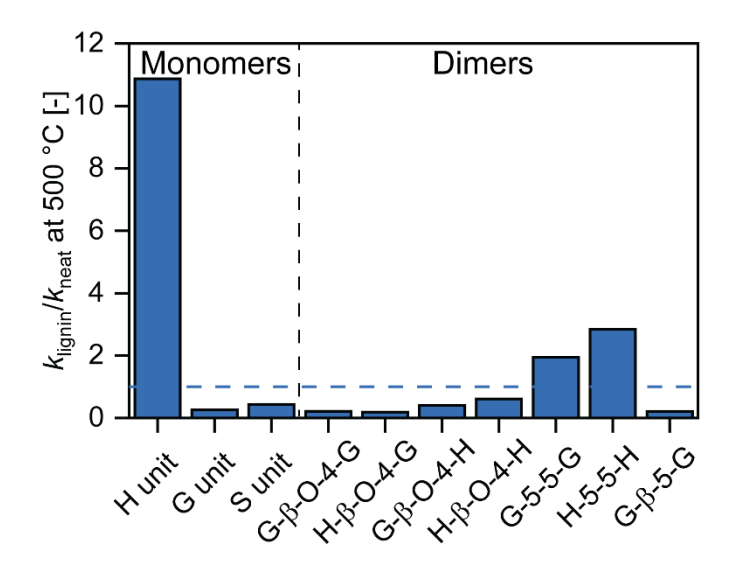


Figure 1. DFT-calculated relative rate constants $k_{\text{lignin}}/k_{\text{neat}}$ of CE glycosidic bond cleavage leading to levoglucosan formation in the presence of monomeric and dimeric lignin surrogates at 500°C.

The three most common linkages (viz., β -O-4, β -5, and 5-5 shown in **Figure S3b**) were also selected to elucidate the effect of different lignin structures on glycosidic bond cleavage during cellulose pyrolysis. The presence of lignin dimers with β -O-4 and β -5 linkages were found to cause an inhibitory effect on CE glycosidic bond cleavage, as opposed to a catalytic effect induced by dimers with a 5-5 linkage. Since dimers with β -O-4 and β -5 linkages have ether bonds, which do not exist in the 5-5 linkages, (**Figure S3b**), they represent another example of ether-induced NCIs inhibiting CE glycosidic bond cleavage.

A closer examination on the different combinations of H and G units (selected for catalytic and inhibitory effect, respectively) connecting β -O-4 and 5-5 linkages reveal that the types of lignin linkages are more critical in determining the resulting stabilizing or destabilizing effect than the

individual unit types they are connecting to. In the case of dimers with a β -O-4 linkage, although the presence of H- β -O-4-H leads to an increase of 2.8 times in the rate constant ($k_{\text{H-}\beta\text{-O-4-H}}/k_{\text{neat}}$ =0.6) compared to that of G- β -O-4-G ($k_{\text{G-}\beta\text{-O-4-G}}/k_{\text{neat}}$ =0.2), the net effect on CE glycosidic bond cleavage caused by β -O-4 linkages is still inhibitory ($k_{\text{lignin}}/k_{\text{neat}}$ <1). A similar trend was also observed for dimers with a 5-5 linkage. The presence of G-5-5-G leads to a decrease of 0.7 times in the rate constant ($k_{\text{G-5-5-G}}/k_{\text{neat}}$ =1.9) compared to that of H-5-5-H ($k_{\text{H-5-5-H}}/k_{\text{neat}}$ =2.8), while the net effect on CE glycosidic bond cleavage caused by 5-5 linkages is still catalytic ($k_{\text{lignin}}/k_{\text{neat}}$ >1).

Our initial DFT screening paints a consistent molecular picture of how the complexity and variability of the nearby lignin structures dictate the reactivity of CE pyrolysis. To allow our study to focus on the NCI effects induced by lignin linkages, two lignin surrogates (i.e., G-β-O-4-G and H-5-5-H) were selected for microreactor experiments and additional DFT calculations to further explore their catalytic or inhibitory effects on CE pyrolysis. The choice of these two lignin linkages was based on two factors: (1) their abundance in native biomass, and (2) their potential impact on CE glycosidic bond cleavage, the main CE pyrolysis pathway, based on our initial screening using DFT (**Figure 1**). G monolignols and β -O-4 linkages invariably represent the most abundant monomer unit and structural linkage in native biomass (Table 1). Our initial DFT screening also shows that β-O-4 clearly induces an inhibitory effect on CE glycosidic bond cleavage regardless the monomers connected (**Figure 1**). As a result, G-β-O-4-G was chosen as a surrogate to represent C-O linkages in lignin. Similarly, the 5-5 linkage was chosen to represent C-C linkages due to its abundance in native biomass (**Table 1**) and its potential catalytic effect on CE pyrolysis based on our initial DFT screening (**Figure 1**). The choice of H-5-5-H as a surrogate, as opposed to G-5-5-G or G-5-5-H, was due to its higher potential to induce catalytic effects (Figure 1) and its availability to purchase so that there is no need to synthesize the compound in the lab.

Co-pyrolysis of cellulose (CE) and lignin dimers. The mass yields of CE-derived products obtained from neat CE pyrolysis and co-pyrolysis of CE with C28, G-β-O-4-G, or H-5-5-H (denoted as CE+C28, CE+G-β-O-4-G, or CE+H-5-5-H, respectively) are shown in Figure 2a. All detected products obtained from neat CE pyrolysis and their corresponding carbon yields are given in Table S2. Note that no products were observed from neat C28 or G-β-O-4-G pyrolysis, and all the initial C28 and G-β-O-4-G mass preloaded to the reactor were recaptured in the condenser after the neat pyrolysis experiments, suggesting that C28 and G-β-O-4-G vaporized and transported to the condenser without decomposition at this reaction temperature (500°C). Neat H-5-5-H pyrolysis only produced 8.5 wt% of dibenzofuran, distinct from CE-derived pyrolysis products, while the remainder of the initial H-5-5-H mass was also recaptured in the condenser due to vaporization. Since C28 has a similar volatility (a boiling point of 432°C at 1 atm) to the lignin dimers studied, the CE+C28 experiment was chosen as the control for the co-pyrolysis experiments to account for the inhibition of anhydrosugar oligomers escape due to the presence of molten lignin dimers before they vaporized.³⁶

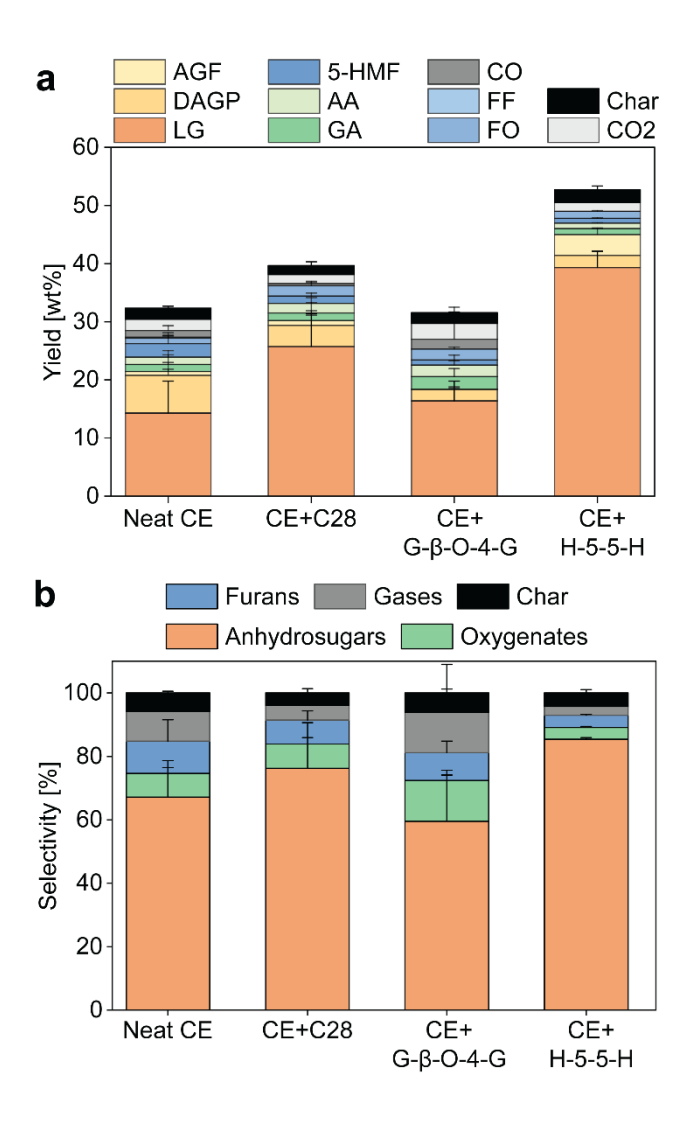


Figure 2. (a) Mass yields of CE-derived products and (b) selectivity toward CE-derived anhydrosugars, small oxygenates, furans, gases, and char from neat CE pyrolysis and co-pyrolysis of CE with C28 (CE+C28), G-β-O-4-G (CE+G-β-O-4-G), or H-5-5-H (CE+H-5-5-H). Mass yields are shown for levoglucosan (LG), dianhydroglucopyranose (DAGP), 1,6-anhydroglucofuranose (AGF), glycolaldehyde (GA), acetic acid (AA), 5-hydroxymethylfurfural (5-HMF), 2-(5H)-furanone (FO), furfural (FF), carbon monoxide (CO), carbon dioxide (CO₂), and char. Reaction condition: 5.0, 2.60, 4.05, and 4.25 mg of CE, C28, G-β-O-4-G, and H-5-5-H, respectively, at 500°C under vacuum.

In our work, all co-pyrolysis experiments resulted in the same products as those from the neat pyrolysis of individual components. No new products from the coupling of individual component pyrolysis were detected (which, if present, would contain structures derived from both feedstocks within a molecule that could have been detected by GC). Specifically, all the initial C28 and G-β-O-4-G mass preloaded to the reactor was again recaptured in the condenser without decomposition after their respective co-pyrolysis with CE. This suggests that β -O-4 linkages in actual lignin have a longer decomposition timescale than CE during pyrolysis. For H-5-5-H co-pyrolysis with CE, a slightly higher dibenzofuran yield (9.6 wt%) was observed, with the remainder of the initial H-5-5-H mass again recaptured in the condenser. This suggests that C28, G-β-O-4-G, and H-5-5-H did not actively participate in the reactions during their respective co-pyrolysis with CE. Distributions (i.e., yields and selectivity) of the CE-derived products from the co-pyrolysis experiments, however, were significantly shifted, with all three sets of co-pyrolysis experiments (CE+C28, CE+G-β-O-4-G, and CE+H-5-5-H) presenting distinct product distributions. Since the binary samples used for co-pyrolysis experiments were simply mixed and melted, no covalent interactions between the components were expected. The differences in product distributions between the three sets of co-pyrolysis experiments can thus only be attributed to selected CE decomposition pathways being catalyzed (accelerated) or inhibited (decelerated) by the NCIs induced by the lignin moieties.²³

The LG yield from our thin-film neat CE pyrolysis experiment was 14.3 wt%. This low LG yield is comparable with those reported using a fast-heating (~5,000°C s⁻¹) wire-mesh reactor.³⁷ As discussed in our previous work,²³ the mass balance closure from our neat CE pyrolysis experiments did not reach 100 wt% (**Figure 2a**) due to the formation of anhydrosugar oligomers (e.g., cellobiosan, cellotriosan, cellotetrasan, etc.) and water vapor that were not detectable by GC. Westerhof et al.³⁷ showed that CE pyrolysis near vacuum (at 5 mbar) resulted in increased yields of anhydrosugar oligomers compared to 1 bar due to accelerated escape of anhydrosugar oligomers

via evaporation, thermal ejection, and/or sublimation, preventing them from further decomposition into smaller products.³⁸ Similarly, high yields of anhydrosugar oligomers were expected in our neat CE pyrolysis experiments since they were operated at near vacuum pressures (<0.04 mbar), accounting for the undetected mass.

As suggested in our previous work,³⁶ the presence of molten plastics prolongated evaporation and thermal ejection of anhydrosugar oligomers, aiding their decomposition into LG and LMWPs. As shown in **Figure 2a**, the presence of C28 similarly resulted in increased yields of CE-derived anhydrosugars and LMWPs by 8.9 wt%. The decomposition of anhydrosugar oligomers can be inferred from the reduced undetected mass obtained from CE+C28 experiments. Since C28 is nonpolar, the changes in CE-derived products obtained from the co-pyrolysis between CE and C28 can be only explained by the physical inhibition of anhydrosugar oligomer escape caused by the presence of C28. Since the same sample thickness (228 μm) were used in all binary co-pyrolysis experiments, the degree of inhibition of anhydrosugar escape was assumed to be same. Consequently, comparing CE+G-β-O-4-G or CE+H-5-5-H experiments against CE+C28 experiments presents the best unbiased NCI effects caused by lignin dimers.

Our experiments showed that the presence of lignin dimers had a diverse effect on CE product distributions. The presence of G-β-O-4-G reduced the yields of LG and CE-derived volatiles by 11.7 and 10.9 wt%, respectively, while the presence of H-5-5-H increased the yields of CE-derived volatiles by 12.8 wt%, mainly contributed by an increased LG yield by 14.8 wt%. As shown in our previous study,²³ NCIs between CE and plastics containing different functional groups can alter product distributions from CE pyrolysis. The variations in yields of CE-derived products in the presence of two different lignin dimers could be similarly originated from NCIs induced by lignin

dimers where CE pyrolysis pathways are catalyzed or inhibited through transition-state stabilization.

To further investigate the NCI-induced effects, CE-derived pyrolysis products were grouped into three families: i) anhydrosugars, ii) small oxygenates, and iii) furans, along with gases and char. CE+G-β-O-4-G resulted in markedly decreased selectivity toward anhydrosugars compared to CE+C28 (**Figure 2b**), while CE+H-5-5-H led to increased anhydrosugar selectivity by 9.1 %. CE+G-β-O-4-G also led to increased selectivity toward small oxygenates and furans by 5.7 and 1.2 %, respectively, compared to CE+C28. On the contrary, CE+H-5-5-H led to decreased selectivity toward small oxygenates and furans by 3.9 and 3.7 %, respectively.

In CE fast pyrolysis, char is assumed to be produced from secondary dehydration and bimolecular condensation reactions of volatile products, with a typical range of 5–8 wt% at atmospheric pressure.^{3,22,37} In this work, char obtained from neat CE pyrolysis was only 1.9 wt% (**Figure 2a**). This lower char yield could be attributed to the suppressed aforementioned secondary char formation reactions under vacuum.³⁹ Char obtained from the co-pyrolysis experiments is assumed to be originated only from CE since no char was observed from neat pyrolysis of C28, G-β-O-4-G, or H-5-5-H. Co-pyrolysis experiments yielded about 1.6–2.2 wt% of char, close to 1.9 wt% from neat CE pyrolysis, suggesting that the presence of C28, G-β-O-4-G, or H-5-5-H has negligible effects on char formation.

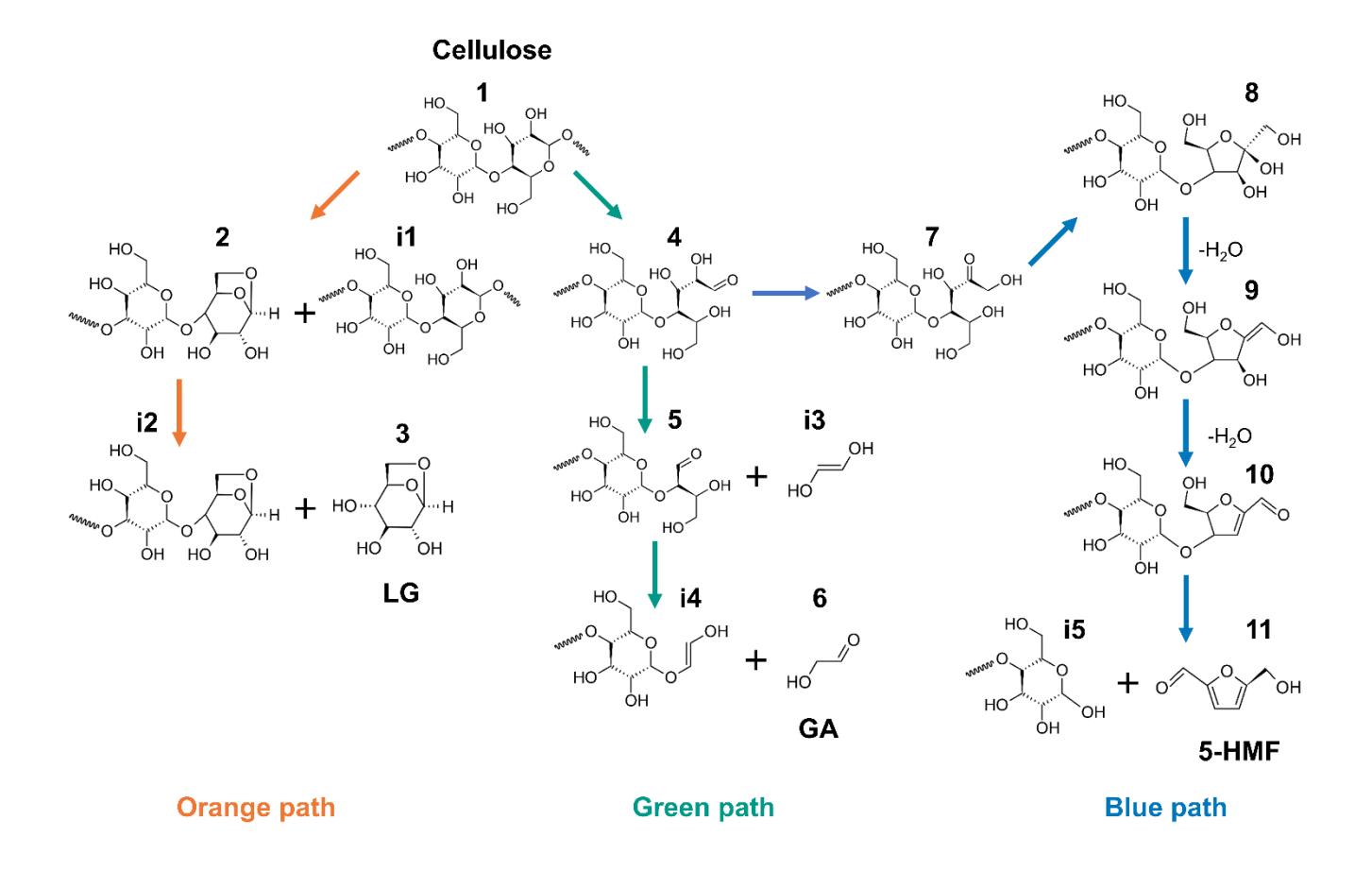
The only gaseous molecules detected from CE pyrolysis were CO and CO₂, with yields of 1 and 2 wt%, respectively. CO and CO₂ obtained from the co-pyrolysis experiments are assumed to be originated from CE because neither molecule was detected from neat pyrolysis of C28, G-β-O-4-G, or H-5-5-H. Co-pyrolysis experiments showed a decreased CO yield by 0.8 wt% in the presence

of C28 and an increased CO yield by 0.6 wt% in the presence of G-β-O-4-G. Notably, no CO formation was observed in the presence of H-5-5-H. The formation of CO and CO₂ is believed to involve a series of complex reactions including decarbonylation and decarboxylation.⁴⁰ Quantum chemistry studies also suggest that the formation of CO₂ starts with acetic acid and formic acid, followed by decarboxylation.⁴¹ As shown in **Figure 2a**, CO₂ and acetic acid yields in our experiments decreased by 0.5 and 0.3 wt% in the presence of H-5-5-H, while they both increased by 0.7 wt% in the presence of G-β-O-4-G. However, this correlation did not hold in the presence of C28, where a decrease in the CO₂ yield by 0.4 wt% was observed in contrast to an increase in the acetic acid yield by 0.4 wt%. It has also been proposed that the formation of CO and CO₂ is also associated with char formation due to secondary decomposition of CE-derived volatiles.^{22,40} Since CO and CO₂ yields were all very small in our experiments, it was difficult to conclude any effects caused by the presence of lignin dimers. More research is needed to understand the formation pathways of CO and CO₂ during CE pyrolysis.

Effect of different lignin motifs on cellulose (CE) pyrolysis. DFT calculations were carried out to address how the presence of lignin motifs impacts CE pyrolysis pathways at the molecular level. Our main objective is to reveal the underlying effects of lignin-induced NCIs on CE pyrolysis. To this end, the major product from each bio-oil product family (LG from anhydrosugars, GA from small oxygenates, and 5-HMF from furans) was selected for further investigation in this study. Although our work showed distinct variations in mass yields of CE-derived products comparing neat CE pyrolysis and co-pyrolysis experiments, no new products were identified (Figure 2a). Consequently, we postulate that reaction pathways of CE pyrolysis remain the same in the presence of lignin dimers, albeit with altered reaction kinetics (i.e., rate constants) due to the possible catalytic and inhibitory effects caused by lignin-induced NCIs. Similar observations were reported

for CE pyrolysis in the presence of thermoplastics containing functional groups in our recent study.²³

Scheme 1 illustrates the major reaction pathways leading to LG (orange path), GA (green path), and 5-HMF (blue path) during CE pyrolysis. The kinetic parameters for the elementary reactions (represented as arrows) were calculated by DFT in our previous work using cellobiose (as a CE surrogate) with and without the presence of C3 (as a polyethylene surrogate).²³ The presence of C3 does not alter the reaction rates investigated at 500°C, leading to an average rate constant ratio (i.e., $k_{\text{C3}}/k_{\text{neat}}$) of 1.01.²³ In this present work, the experimentally observed alteration of CE-derived product distribution from the CE+C28 experiments compared to neat CE pyrolysis was viewed as solely caused by the inhibition of anhydrosugar escape. Given the chemical similarities between C28 and polyethylene, the same DFT calculations involving C3 can be used to interpret the results from the CE+C28 experiments.



Scheme 1. Elementary steps of CE pyrolysis investigated by DFT, leading to levoglucosan (LG, **3**), glycolaldehyde (GA, **6**), and 5-hydroxymethylfurfural (5-HMF, **11**). Reproduced from Sakirler *et al.* ²³ with permission from the Royal Society of Chemistry.

In our DFT calculations, the reaction pathways shown in **Scheme 1** were studied in the presence of G- β -O-4-G or H-5-5-H. The kinetic parameters at 500°C were determined using the lowest-energy conformers of the reactants and TSs. To better evaluate the lignin-induced catalytic or inhibitory effects, a rate constant ratio (R) is defined as the ratio of the rate constant in the presence of G- β -O-4-G or H-5-5-H (representing CE+G- β -O-4-G or CE+H-5-5-H) to that in the presence of C3 (representing CE+C28):

$$R(i,T) = k_x(i,T)/k_{C3}(i,T)$$
 $x = G-\beta-O-4-G, H-5-5-H$ (1)

where *T* is the reaction temperature. For each elementary step, R>1 represents being catalyzed, and R<1 represents being inhibited.²³

Levoglucosan (LG) formation. Orange path in **Scheme 1** demonstrates the formation pathway of LG (3) during CE pyrolysis, including a mid-chain initiation step followed by an end-chain depolymerization step.²² In this study, C–O cleavage of cellobiose (1), a surrogate for CE, is used to represent mid-chain initiation of CE, leading to "active CE" (i.e., a CE chain with a LG-like end). C–O cleavage of cellobiosan (2) is used to describe end-chain depolymerization of active CE, yielding LG. Our DFT results in the absence of any surrogates showed that the depolymerization (i.e., second) step is rate-limiting, having a higher activation energy of 52.1 kcal mol⁻¹ compared to 48.3 kcal mol⁻¹ from mid-chain initiation.²³

Figure 3a shows the DFT-predicted R values for each elementary step of LG formation in the presence of G-β-O-4-G or H-5-5-H. Both C-O cleavage reactions is inhibited by NCIs induced by G-β-O-4-G, while the presence of H-5-5-H catalyzes both C-O cleavage reactions. To make a qualitative comparison between the experimental and DFT findings, the DFT-predicted R value of the rate-limiting step ($2 \rightarrow 3 + i2$ for LG formation) is compared to the experimental selectivity toward LG (**Figure 3b**). The presence of G-β-O-4-G led to an inhibitory effect on the rate-limiting step ($R_{G-\beta-O-4-G}$ =0.25), matching the qualitative trend (decreased LG selectivity by 11.9 %) observed from the CE+G-β-O-4-G experiment. Likewise, there is a qualitative agreement between the experiments and the DFT-predicted R value for the effects of H-5-5-H. The presence of H-5-5-H resulted in a catalytic effect on the rate-limiting step ($R_{H-5-5-H}$ =3.3), which is supported by the enhanced LG selectivity by 9.7 % observed from the CE+H-5-5-H experiments.

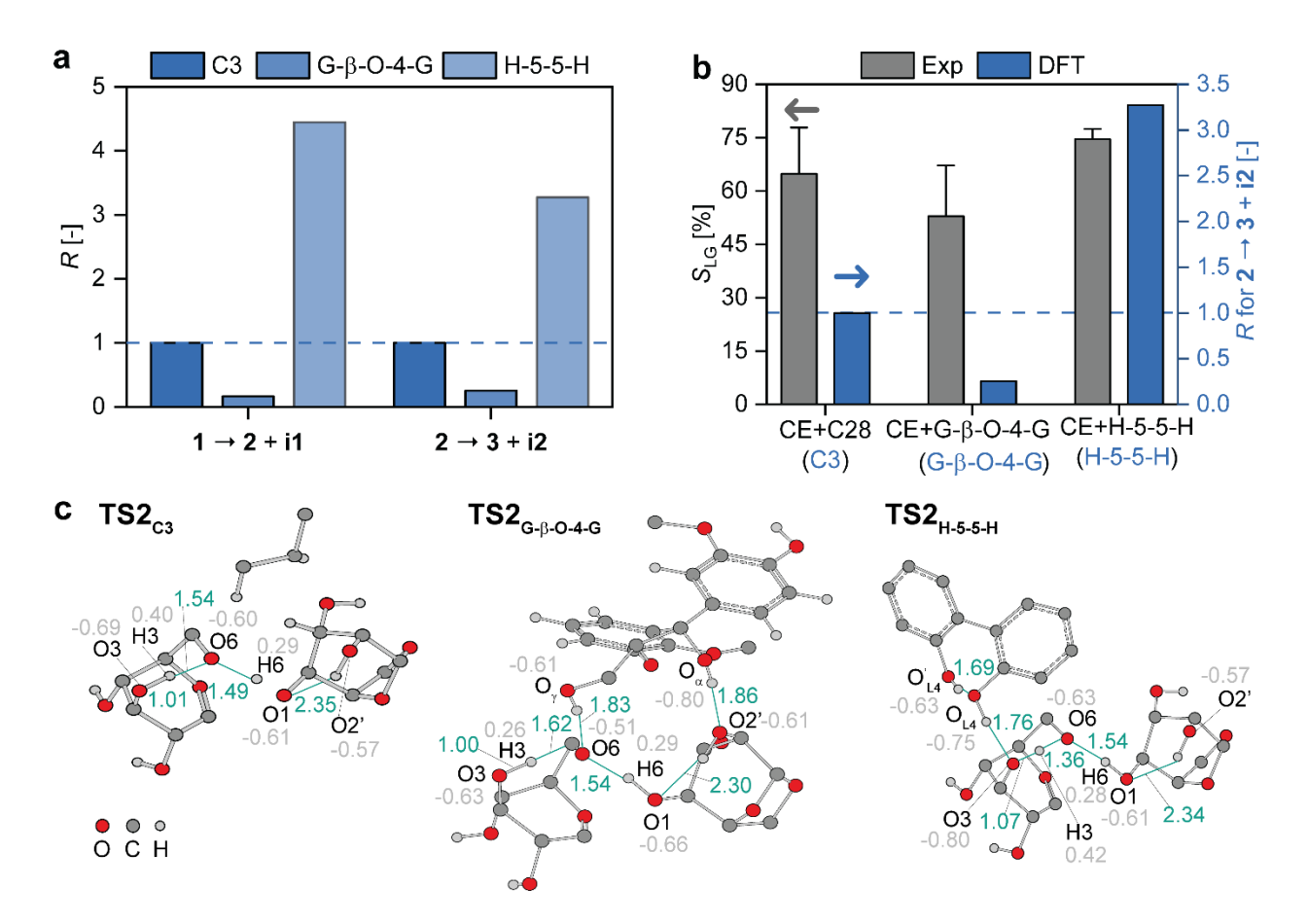


Figure 3. (a) DFT-calculated rate constant ratios (R) of the elementary steps leading to levoglucosan (LG) formation in the presence of C3, G-β-O-4-G, or H-5-5-H at 500°C. (b) Comparison of experimental selectivity toward LG from CE+C28, CE+G-β-O-4-G, or CE+H-5-5-H against the DFT-calculated R values for the rate-limiting step ($\mathbf{2} \rightarrow \mathbf{3} + \mathbf{i2}$) of LG formation. (c) TSs for the rate-limiting step in the presence of C3, G-β-O-4-G, or H-5-5-H including key distances and partial charges. Numbers in green and grey represent distances in Å and ChelpG partial charges in au, respectively. Hydrogen atoms not involved in noticeable interactions are omitted for clarity.

Previous experimental and DFT studies^{23,25,32-35} have demonstrated that hydroxyl functional groups near the reaction center of C–O cleavage during CE pyrolysis can perturb electronic properties of charge-separated TSs *via* NCIs, resulting in more stabilized TSs and lower reaction barriers. Here, even though hydroxyl groups of both G-β-O-4-G and H-5-5-H donate hydrogen bonds to

cellobiosan (2), the resulting effect on the rate-limiting step of LG formation is opposite (**Figure 3c**). In the presence of G- β -O-4-G, transition-state destabilization is attributed to the steric effect caused by the ether groups of G- β -O-4-G, including those of the G units. Our DFT calculations indicate that **TS2**_{G- β -O-4-G} has partial charges of -0.51 and -0.63 au, respectively, on the O6 and O3 atoms. These values are less than those from **TS2**_{C3} by 0.09 and 0.06 au, respectively. In addition, **TS2**_{G- β -O-4-G} has a partial charge of 0.26 au on the H6 atom, which is less than that of **TS2**_{C3} by 0.14 au. These changes in partial charges make **TS2**_{G- β -O-4-G} less susceptible to nucleophilic attack during C-O cleavage than **TS2**_{C3}. Moreover, the O3-H···O6 intramolecular hydrogen bond of **TS2**_{G- β -O-4-G} is elongated by 0.08 Å compared to **TS2**_{C3}, indicating reduced hydrogen bond strength and TS stability. Additional intermolecular hydrogen bonds to the O6 and O2' atoms are not strong enough to overcome the steric effects caused by the ether groups (see **TS2**_{G- β -O-4-G} in **Figure 3c**, O₇-H···O6, 1.83 Å; O₆-H···O2', 1.86 Å).

On the other hand, H-5-5-H induces a catalytic effect on the rate-limiting step of LG formation, which is originated by a new intermolecular hydrogen bond (stronger than those of TS2_{G-β-O-4-G}) to the O3 atom (see TS2_{H-5-5-H} in Figure 3c, O_{L4}–H···O3, 1.76 Å). In addition, the presence of H-5-5-H results in perturbations of atomic distances and partial charges. For instance, the O3–H···O6 hydrogen bond is shorten by 0.18 Å and the distance between O3 and O3–H of TS2_{H-5-5-H} is elongated by 0.06 Å compared to TS2_{C3}, leading to transition-state stabilization through a stronger hydrogen bond. The increased hydrogen bond strength can be inferred by more negative charges on the O3 and O6 atoms of TS2_{H-5-5-H} than those of TS2_{C3} by 0.11 and 0.03 au, respectively, and more positive charges on O3-H of TS2_{H-5-5-H} than those of TS2_{C3} by 0.02 au.

Glycolaldehyde (GA) formation. Green path in **Scheme 1** portrays GA (6) formation during CE pyrolysis. Experimental^{42,43} and theoretical^{41,44} findings lend direct support to the hypothesis that GA formation originates from the reducing end of CE chains. In this study, the formation of GA is studied by DFT by starting with ring opening of the reducing end of cellobiose (1), yielding an acyclic glucose-end cellobiose (4). GA (6) is eliminated from the reducing end *via* two consecutive retro-aldol reactions through an aldose intermediate (5). Our DFT calculations in the absence of any lignin surrogates show that ring opening $(1 \rightarrow 4)$ is the rate-limiting step with an activation energy of 48.0 kcal mol⁻¹, compared to 36.3 and 32.9 kcal mol⁻¹ for the two retro-aldol condensation reactions $(4 \rightarrow 5 + i3, 5 \rightarrow 6 + i4)$.²³

Figure 4a demonstrates the DFT-predicted R values for each elementary step of GA formation in the presence of G-β-O-4-G or H-5-5-H. The ring opening ($R_{G-\beta-O-4-G}=1.35$) and the first retro-aldol condensation ($R_{G-\beta-O-4-G}=12.8$) reactions are catalyzed by G-β-O-4-G-induced NCIs, while the second retro-aldol condensation reaction ($R_{G-\beta-O-4-G}=0.11$) is inhibited. On the other hand, each elementary step in GA formation is inhibited by H-5-5-H, with the most significant effect on the first retro-aldol condensation reaction ($R_{H-5-5-H}=0.18$).

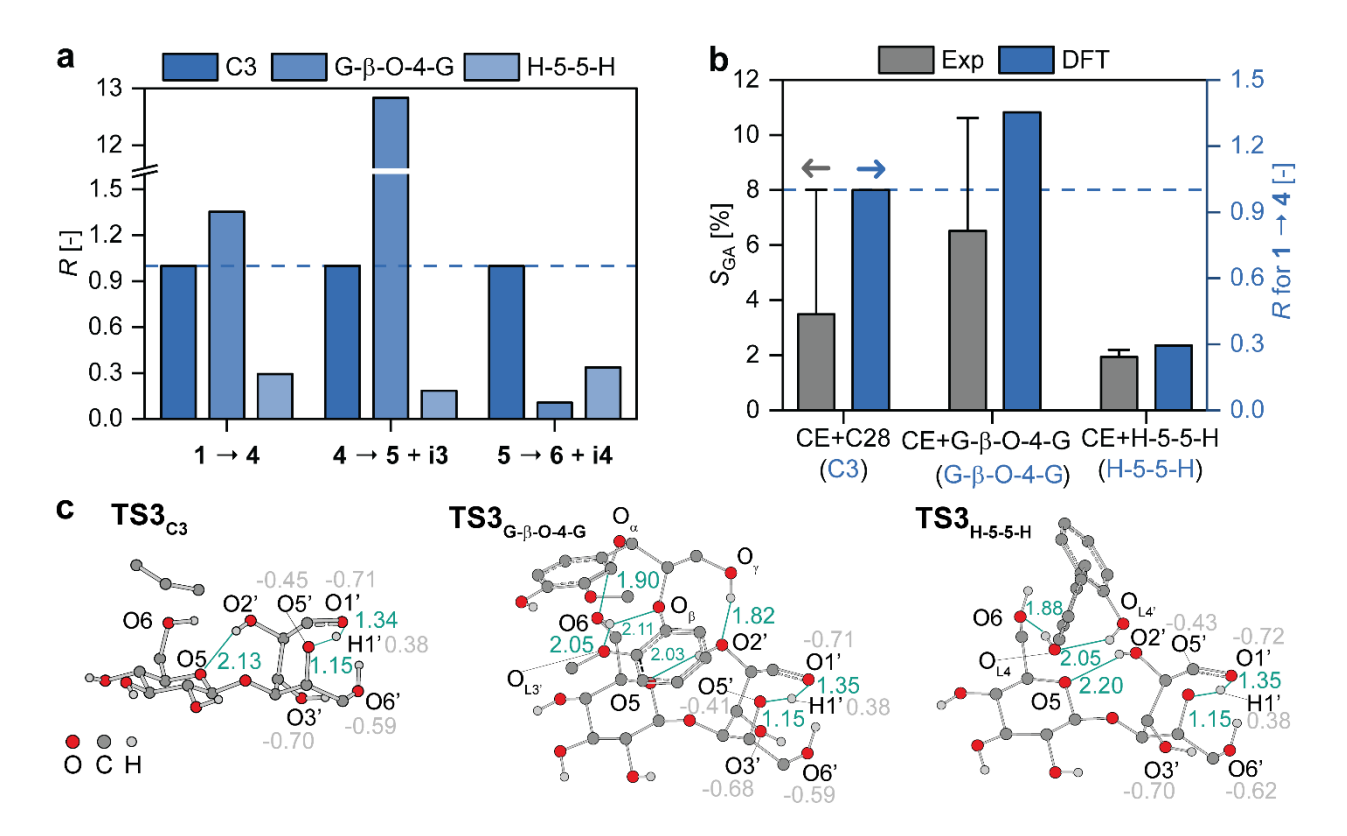


Figure 4. (a) DFT-calculated rate constant ratios (R) of the elementary steps leading to glycolaldehyde (GA) formation in the presence of C3, G-β-O-4-G, or H-5-5-H at 500°C. (b) Comparison of experimental selectivity toward GA from CE+C28, CE+G-β-O-4-G, or CE+H-5-5-H against the DFT-calculated R values for the rate-limiting step ($1 \rightarrow 4$) of GA formation. (c) TSs for the rate-limiting step in the presence of C3, G-β-O-4-G, or H-5-5-H including key distances and partial charges. Numbers in green and grey represent distances in Å and ChelpG partial charges in au, respectively. Hydrogen atoms not involved in noticeable interactions are omitted for clarity.

Our DFT-predicted R values of the rate limiting step qualitatively agree well with the experimental trends in the presence of lignin dimers (**Figure 4b**). The presence of G- β -O-4-G led to a catalytic effect on the rate-limiting step ($R_{G-\beta-O-4-G}=1.35$), matching the enhanced selectivity toward GA about 3 %. The presence of H-5-5-H resulted in an inhibitory effect on the rate-limiting step ($R_{H-5-5-H}=0.29$), which is supported by the decreased selectivity toward GA by 1.7 % from CE+H-5-5-H.

The presence of G-β-O-4-G or H-5-5-H leads to several convoluted intermolecular hydrogen bonds as opposed to none in the presence of C3 (Figure 4c). For instance, the O6 hydroxyl group of 1 forms a bifurcated hydrogen bond to the O β and O_{L3} atoms of G- β -O-4-G. In addition, the O α and Oy atoms of G-β-O-4-G each forms a hydrogen bond to the O6 and O2' atoms of 1, respectively. On the other hand, the $O_{1.4}$ atom of H-5-5-H donates a hydrogen bond to the O6 atom of 1, while the O2' atom of 1 forms a hydrogen bond to the O_{L4}' atom of H-5-5-H. However, there were no more than 0.04 au perturbations in partial charges on the atoms, such as O1', H1', O3', O5', and O6'. In addition, changes of distances between O1'...H1' and O5'...H1' near the reaction center were no more than 0.01 Å. Even though these new intermolecular hydrogen bonds in the presence of G-β-O-4-G or H-5-5-H are not located near the reaction center, it was found that lignin dimers still influence the TSs of the ring opening reaction. Specifically, the O2'-H···O5 intramolecular hydrogen bond of TS3_{G-B-O-4-G} are shortened by 0.10 Å compared to TS3_{C3}, indicating increased hydrogen bond strength and TS stability ($R_{G-\beta-O-4-G}=1.35$). In contrast to the presence of G- β -O-4-G, the O2'-H···O5 intramolecular hydrogen bond of TS3_{H-5-5-H} is elongated by 0.07 Å compared to $TS3_{C3}$, indicating reduced hydrogen bond strength and decreased steric stabilization (R_{H-5-5} H=0.29).

5-Hydroxymethylfurfural (5-HMF) formation. In this work, the reaction pathways leading to 5-HMF are studied by DFT *via* a fructose-end intermediate^{45,46} (depicted as "blue path" in **Scheme**1). First, cellobiose (1) yields an acyclic glucose-end cellobiose (4) *via* ring opening, followed by isomerization of 4 to an acyclic fructose-end cellobiose (7). This intermediate undergoes ring closing to form a fructose-end intermediate (8), which undergoes dehydration to produce an enolend intermediate (9). A second dehydration of 9 occurs to form a dihydrofuran-end intermediate (10), which undergoes C–O cleavage to form a glucose (i5) and 5-HMF (11). Our DFT calculations

in the absence of any surrogates suggest that the first dehydration reaction (8 \rightarrow 9 + H₂O) is the rate-limiting step with an activation energy of 70.1 kcal mol⁻¹.²³

Figure 5a demonstrates the DFT-predicted *R* values for each elementary step of 5-HMF formation in the presence of G-β-O-4-G or H-5-5-H. Both lignin dimers inhibit isomerization (4 → 7) and the first dehydration reaction, whereas they catalyze ring closing (7 → 8), the second dehydration reaction (9 → 10 + H₂O), and C-O cleavage (10 → 11 + i5). However, the extent of catalytic or inhibitory effects on the elementary steps of 5-HMF formation is different. For instance, the inhibitory effect on isomerization 4 → 7 induced by H-5-5-H ($R_{\text{H-5-5-H}}$ =0.01) is approximately 60 times larger than that induced by G-β-O-4-G ($R_{\text{G-\beta-O-4-G}}$ =0.61). On the other hand, the catalytic effect on ring closing 7 → 8 induced by H-5-5-H ($R_{\text{H-5-5-H}}$ =7.37) is 5.3 times larger than that induced by G-β-O-4-G ($R_{\text{G-\beta-O-4-G}}$ =1.39).

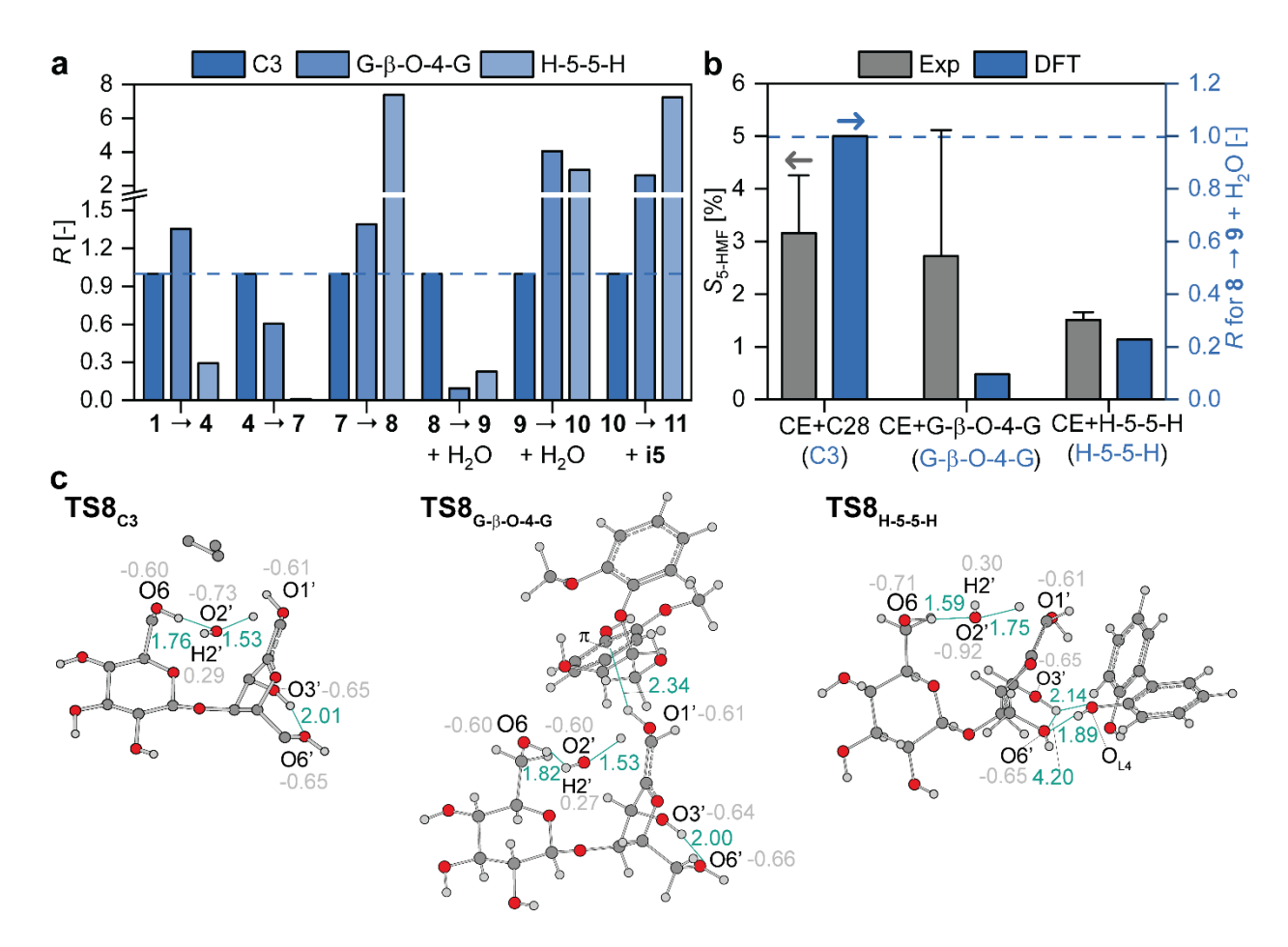


Figure 5. (a) DFT-calculated rate constant ratios (R) of the elementary steps of 5-hydroxymethylfurfural (5-HMF) formation in the presence of C3, G-β-O-4-G, or H-5-5-H at 500°C. (b) Comparison of experimental selectivity toward 5-HMF from CE+C28, CE+G-β-O-4-G, or CE+H-5-5-H against the DFT-calculated R values for the rate-limiting step ($\mathbf{8} \rightarrow \mathbf{9} + \text{H}_2\text{O}$) of 5-HMF formation. (c) TSs for the rate-limiting step in the presence of C3, G-β-O-4-G, or H-5-5-H including key distances and partial charges. Numbers in green and grey represent distances in Å and ChelpG partial charges in au, respectively. Hydrogen atoms not involved in noticeable interactions are omitted for clarity.

Our DFT-predicted R values of the rate limiting step in 5-HMF formation qualitatively captures the experimental trends in the presence of G- β -O-4-G or H-5-5-H as shown in **Figure 5b**. The presence of G- β -O-4-G or H-5-5-H leads to an inhibitory effect on the rate-limiting step ($R_{G-\beta}$ -O-4-

 $_{\rm G}$ =0.23, $R_{\rm H\text{-}5\text{-}5\text{-}H}$ =0.10), which is supported by the decreased selectivity toward 5-HMF by 0.40 and 0.47 % from CE+G-β-O-4-G and CE+H-5-5-H, respectively.

The structural and electrostatic investigation of TSs for the first dehydration reaction (8 \rightarrow 9 $^+$ H_2O) reveals that hydroxyl-rich G-β-O-4-G leads to a single O-H···π hydrogen bond with a fructose-end cellobiose (8) as shown in Figure 5c. On the contrary, the O_{L4} atom of H-5-5-H acts not only as a donor, but also as an acceptor for a stronger O-H···O type hydrogen bond compared to the O-H··· π type hydrogen bond. It was also found that **TS8**_{G-B-O-4-G} has 0.13 au less negative and 0.02 au less positive partial charges on the O2' and H2' atoms, respectively, compared to those of TS8_{C3} (partial charges of -0.73 and 0.29 au, respectively). Thus, the presence of G-β-O-4-G results in an inhibitory effect on this rate-limiting dehydration step (8 \rightarrow 9 + H₂O), suggesting that the O1'-H $\cdots\pi$ intermolecular hydrogen bond alone does not compensate destabilizing NCIs. On the other hand, our DFT calculations show that TS8_{H-5-5-H} has 0.19 au more negative and 0.01 au more positive partial charges on the O2' and H2' atoms, respectively, compared to those of TS8_{C3}, suggesting stabilizing NCIs. Given a more favorable electronic structure and two intermolecular hydrogen bonds between H-5-5-H and 8 (O_{L4}-H···O6', O3'-H···O_{L4}), the presence of H-5-5-H elongates the atomic distance between the O3' hydroxyl group and O6' by 2.19 Å compared to that of TS8_{C3}, invoking steric hinderance on the O3'-H··· O6' intramolecular hydrogen bond in TS8_{C3}. This illustrates an example where competing stabilizing and destabilizing NCIs can act in concert to affect the overall energetic stability of the TSs.

Insights into cellulose–lignin interactions on levoglucosan (LG) formation. Although the results presented in this work only elucidate molecular-level interactions between cellobiose and lignin dimers, they carry general implications on pyrolysis of actual biomass feedstocks. Numerous studies observed catalytic or inhibitory effects on LG formation from co-pyrolysis of native or

hand-mixed CE-lignin mixtures. 18,19,47,48 Drawing from the knowledge of these studies and our results in Section 3.3.1, the inhibitory effect caused by G-β-O-4-G can help elucidate why reduced LG yields are typically observed from the pyrolysis of biomass containing herbaceous lignin, such as corn stover and switchgrass, 47 in which β-O-4 is the most abundant linkage (**Table 1**). On the other hand, the catalytic effect caused by H-5-5-H may explain enhanced LG formation observed from the pyrolysis of biomass containing wood lignin, such as cedar wood (softwood), 18 pine (softwood), and red oak (hardwood), 47 in which there is increased C-C linkages at the expense of β-O-4 linkages (**Table 1**).

Most of C–O linkages in native lignin, such as β -O-4, are cleaved during lignin fractionation in biorefineries. Thus, the structure of extracted lignin is significantly altered, leading to more C-C linkages, such as 5-5 or alkyl linkages, in organosolv lignin.⁶ Hence, enhanced LG formation observed from organosolv lignin pyrolysis^{19,48} can be attributed to the elevated presence of C-C linkages, similar to the effects of H-5-5-H revealed in this study.

Our work indicates that the nature of the synergistic effect between the biomass constituents during actual biomass pyrolysis is dependent on lignin structures and compositions, including functional groups, linkages, and aromatic contents, particularly how CE and lignin interface with each other. These biomass characteristics may be tailored to alleviate the low selectivity challenge facing biomass fast pyrolysis, particularly with the help of genetically engineered plants and pretreatments. 49-51 Machine learning approaches to obtain correlations between biomass structures and product yields from whole biomass pyrolysis are also needed. 52,53

Conclusions

Combined microreactor experiments and DFT calculations unveiled the molecular-level picture of CE–lignin interactions during pyrolysis. Dimeric lignin model compounds induce more dominant effects on product yields than monomers. Our work suggests that β -O-4 linkages caused an inhibitory effect on the levoglucosan and 5-hydroxymethylfurfural formation pathways and a catalytic effect on the glycolaldehyde formation pathway during CE pyrolysis. On the other hand, 5-5 linkages resulted in a catalytic effect on levoglucosan formation and an inhibitory effect on 5-hydroxymethylfurfural and glycolaldehyde formation. These outcomes were attributed to the NCIs induced by lignin hydroxyl and ether motifs that alter the transition states of the rate-determining steps, ultimately influencing CE pyrolysis kinetics. Although lignin also undergoes decomposition at the same time, these catalytic and inhibitory effects should still apply as long as these lignin motifs are present near cellulose in the reaction system.

Supporting Information

Schematic representation of the experimental setup; mass and carbon yields of cellulose-derived products; structures of dimeric lignin surrogates; kinetic parameters and rate constant ratios for each elementary step; calculated relative energies of reactants and TSs.

Acknowledgements

This work was supported by the National Science Foundation CAREER Program (Award Number CBET-1847289) and completed in part with resources provided by the University of Massachusetts' Green High Performance Computing Cluster (GHPCC).

Notes

The authors declare no competing financial interest.

References

- International Energy Agency (IEA) Bioenergy, Paris, 2022.
 https://www.iea.org/reports/bioenergy (accessed 2023-08-02)
- Sharifzadeh, M.; Sadeqzadeh, M.; Guo, M.; Borhani, T. N.; Murthy Konda, N. V. S. N.;
 Garcia, M. C.; Wang, L.; Hallett, J.; Shah, N., The Multi-Scale Challenges of Biomass Fast
 Pyrolysis and Bio-Oil Upgrading: Review of the State of Art and Future Research Directions.
 Prog. Energy Combust. Sci. 2019, 71, 1-80. DOI: https://doi.org/10.1016/j.pecs.2018.10.006
- 3. Mettler, M. S.; Vlachos, D. G.; Dauenhauer, P. J., Top Ten Fundamental Challenges of Biomass Pyrolysis for Biofuels. *Energy Environ. Sci.* **2012**, *5* (7), 7797-7809. DOI: 10.1039/C2EE21679E
- 4. Ranzi, E.; Debiagi, P. E. A.; Frassoldati, A., Mathematical Modeling of Fast Biomass Pyrolysis and Bio-Oil Formation. Note I: Kinetic Mechanism of Biomass Pyrolysis. *ACS Sustainable Chem. Eng.* **2017**, *5* (4), 2867-2881. DOI: 10.1021/acssuschemeng.6b03096
- 5. Jarvis, M. C., Hydrogen Bonding and Other Non-Covalent Interactions at the Surfaces of Cellulose Microfibrils. *Cellulose* **2023**, *30* (2), 667-687. DOI: 10.1007/s10570-022-04954-3
- Lahive, C. W.; Kamer, P. C. J.; Lancefield, C. S.; Deuss, P. J., An Introduction to Model Compounds of Lignin Linking Motifs; Synthesis and Selection Considerations for Reactivity Studies. *ChemSusChem* 2020, 13 (17), 4238-4265. DOI: https://doi.org/10.1002/cssc.202000989
- 7. Zakzeski, J.; Bruijnincx, P. C. A.; Jongerius, A. L.; Weckhuysen, B. M., The Catalytic Valorization of Lignin for the Production of Renewable Chemicals. *Chem. Rev.* **2010**, *110* (6), 3552-3599. DOI: 10.1021/cr900354u
- 8. Lourenço, A.; Pereira, H., Compositional Variability of Lignin in Biomass. In *Lignin Trends and Applications*, Matheus, P., Ed. IntechOpen: Rijeka, **2017**; 65-98.

- Hirayama, H.; Akiyama, T.; Kimura, S.; Nawawi, D. S.; Syafii, W.; Yokoyama, T.; Matsumoto, Y., Influence of the P-Hydroxyphenyl/Guaiacyl Ratio on the Biphenyl and B-5 Contents in Compression Wood Lignins. *Holzforschung* 2019, 73 (10), 923-935. DOI: doi:10.1515/hf-2019-0012
- Neiva, D. M.; Rencoret, J.; Marques, G.; Gutiérrez, A.; Gominho, J.; Pereira, H.; del Río, J. C., Lignin from Tree Barks: Chemical Structure and Valorization. *ChemSusChem* 2020, 13 (17), 4537-4547. DOI: https://doi.org/10.1002/cssc.202000431
- 11. Zeng, J.; Helms, G. L.; Gao, X.; Chen, S., Quantification of Wheat Straw Lignin Structure by Comprehensive Nmr Analysis. *J. Agric. Food. Chem.* **2013**, 61 (46), 10848-10857. DOI: 10.1021/jf4030486
- 12. Wheeler, S. E.; Seguin, T. J.; Guan, Y.; Doney, A. C., Noncovalent Interactions in Organocatalysis and the Prospect of Computational Catalyst Design. *Acc. Chem. Res.* **2016**, 49 (5), 1061-1069. DOI: 10.1021/acs.accounts.6b00096
- 13. Neel, A. J.; Hilton, M. J.; Sigman, M. S.; Toste, F. D., Exploiting Non-Covalent Π Interactions for Catalyst Design. *Nature* **2017**, *543* (7647), 637-646. DOI: 10.1038/nature21701
- Wang, S.; Dai, G.; Yang, H.; Luo, Z., Lignocellulosic Biomass Pyrolysis Mechanism: A State-of-the-Art Review. *Prog. Energy Combust. Sci.* 2017, 62, 33-86. DOI: https://doi.org/10.1016/j.pecs.2017.05.004
- 15. Lin, F.; Waters, C. L.; Mallinson, R. G.; Lobban, L. L.; Bartley, L. E., Relationships between Biomass Composition and Liquid Products Formed Via Pyrolysis. *Front. Energy Res.* **2015**, *3:45*. DOI: 10.3389/fenrg.2015.00045
- 16. Bielecki, M.; Zubkova, V., Analysis of Interactions Occurring During the Pyrolysis of Lignocellulosic Biomass. *Molecules* **2023**, *28* (2), 506. DOI: 10.3390/molecules28020506

- 17. Barr, M. R.; Volpe, R.; Kandiyoti, R., Identifying Synergistic Effects between Biomass Components During Pyrolysis and Pointers Concerning Experiment Design. *ACS Sustainable Chem. Eng.* **2021**, *9* (16), 5603-5612. DOI: 10.1021/acssuschemeng.1c00051
- Hosoya, T.; Kawamoto, H.; Saka, S., Cellulose–Hemicellulose and Cellulose–Lignin Interactions in Wood Pyrolysis at Gasification Temperature. *J. Anal. Appl. Pyrolysis* 2007, 80
 (1), 118-125. DOI: https://doi.org/10.1016/j.jaap.2007.01.006
- Hilbers, T. J.; Wang, Z.; Pecha, B.; Westerhof, R. J. M.; Kersten, S. R. A.; Pelaez-Samaniego, M. R.; Garcia-Perez, M., Cellulose-Lignin Interactions During Slow and Fast Pyrolysis. *J. Anal. Appl. Pyrolysis* 2015, 114, 197-207. DOI: https://doi.org/10.1016/j.jaap.2015.05.020
- 20. Yang, H.; Liu, M.; Chen, Y.; Xin, S.; Zhang, X.; Wang, X.; Chen, H., Vapor–Solid Interaction among Cellulose, Hemicellulose and Lignin. *Fuel* 2020, 263, 116681. DOI: https://doi.org/10.1016/j.fuel.2019.116681
- 21. Wu, K.; Yang, K.; Zhu, Y.; Luo, B.; Chu, C.; Li, M.; Zhang, Y.; Zhang, H., The Co-Pyrolysis Interactionsof Isolated Lignins and Cellulose by Experiments and Theoretical Calculations. *Energy* **2023**, *263*, 125811. DOI: https://doi.org/10.1016/j.energy.2022.125811
- 22. Zhou, X.; Nolte, M. W.; Mayes, H. B.; Shanks, B. H.; Broadbelt, L. J., Experimental and Mechanistic Modeling of Fast Pyrolysis of Neat Glucose-Based Carbohydrates. 1. Experiments and Development of a Detailed Mechanistic Model. *Ind. Eng. Chem. Res.* 2014, 53 (34), 13274-13289. DOI: 10.1021/ie502259w
- Sakirler, F.; Tekbas, M. D.; Wong, H.-W., Molten Plastics Induced Noncovalent Interactions for Tunable Cellulose Fast Pyrolysis. *Green Chem.* 2023, 25 (23), 10010-10019. DOI: 10.1039/D3GC01312J

- 24. Paulsen, A. D.; Mettler, M. S.; Dauenhauer, P. J., The Role of Sample Dimension and Temperature in Cellulose Pyrolysis. *Energy Fuels* 2013, 27 (4), 2126-2134. DOI: 10.1021/ef302117j
- Maduskar, S.; Maliekkal, V.; Neurock, M.; Dauenhauer, P. J., On the Yield of Levoglucosan from Cellulose Pyrolysis. ACS Sustainable Chem. Eng. 2018, 6 (5), 7017-7025. DOI: 10.1021/acssuschemeng.8b00853
- 26. Zhao, Y.; Truhlar, D. G., The M06 Suite of Density Functionals for Main Group Thermochemistry, Thermochemical Kinetics, Noncovalent Interactions, Excited States, and Transition Elements: Two New Functionals and Systematic Testing of Four M06-Class Functionals and 12 Other Functionals. *Theor. Chem. Acc.* 2008, 120 (1), 215-241. DOI: 10.1007/s00214-007-0310-x
- 27. Grimme, S.; Antony, J.; Ehrlich, S.; Krieg, H., A Consistent and Accurate Ab Initio Parametrization of Density Functional Dispersion Correction (DFT-D) for the 94 Elements H-Pu. *J. Chem. Phys.* **2010**, *132* (15), 154104. DOI: 10.1063/1.3382344
- 28. Frisch, M. J.; Trucks, G. W.; Schlegel, H. B.; Scuseria, G. E.; Robb, M. A.; Cheeseman, J. R.; Scalmani, G.; Barone, V.; Petersson, G. A.; Nakatsuji, H.; Li, X.; Caricato, M.; Marenich, A. V.; Bloino, J.; Janesko, B. G.; Gomperts, R.; Mennucci, B.; Hratchian, H. P.; Ortiz, J. V.; Izmaylov, A. F.; Sonnenberg, J. L.; Williams; Ding, F.; Lipparini, F.; Egidi, F.; Goings, J.; Peng, B.; Petrone, A.; Henderson, T.; Ranasinghe, D.; Zakrzewski, V. G.; Gao, J.; Rega, N.; Zheng, G.; Liang, W.; Hada, M.; Ehara, M.; Toyota, K.; Fukuda, R.; Hasegawa, J.; Ishida, M.; Nakajima, T.; Honda, Y.; Kitao, O.; Nakai, H.; Vreven, T.; Throssell, K.; Montgomery Jr., J. A.; Peralta, J. E.; Ogliaro, F.; Bearpark, M. J.; Heyd, J. J.; Brothers, E. N.; Kudin, K. N.; Staroverov, V. N.; Keith, T. A.; Kobayashi, R.; Normand, J.; Raghavachari, K.; Rendell, A. P.; Burant, J. C.; Iyengar, S. S.; Tomasi, J.; Cossi, M.;

- Millam, J. M.; Klene, M.; Adamo, C.; Cammi, R.; Ochterski, J. W.; Martin, R. L.; Morokuma, K.; Farkas, O.; Foresman, J. B.; Fox, D. J. *Gaussian 16*, Rev. C.01; Gaussian, Inc.: Wallingford, CT, 2016.
- Breneman, C. M.; Wiberg, K. B., Determining Atom-Centered Monopoles from Molecular Electrostatic Potentials. The Need for High Sampling Density in Formamide Conformational Analysis. *J. Comput. Chem.* 1990, 11 (3), 361-373. DOI: https://doi.org/10.1002/jcc.540110311
- 30. Grimme, S., Supramolecular Binding Thermodynamics by Dispersion-Corrected Density Functional Theory. *Chem. Eur. J.* **2012,** *18* (32), 9955-9964. DOI: https://doi.org/10.1002/chem.201200497
- 31. Mayes, H. B.; Broadbelt, L. J., Unraveling the Reactions That Unravel Cellulose. *J. Phys. Chem. A* **2012**, *116* (26), 7098-7106. DOI: 10.1021/jp300405x
- 32. Seshadri, V.; Westmoreland, P. R., Roles of Hydroxyls in the Noncatalytic and Catalyzed Formation of Levoglucosan from Glucose. *Catal. Today* **2016**, *269*, 110-121. DOI: https://doi.org/10.1016/j.cattod.2015.10.033
- 33. Sakirler, F.; Wong, H.-W., Cellulose Fast Pyrolysis Activated by Intramolecular Hydrogen Bonds. *J. Phys. Chem. A* **2022**, *126* (43), 7806-7819. DOI: 10.1021/acs.jpca.2c03669
- 34. Maliekkal, V.; Maduskar, S.; Saxon, D. J.; Nasiri, M.; Reineke, T. M.; Neurock, M.; Dauenhauer, P., Activation of Cellulose Via Cooperative Hydroxyl-Catalyzed Transglycosylation of Glycosidic Bonds. ACS Catal. 2019, 9 (3), 1943-1955. DOI: 10.1021/acscatal.8b04289
- 35. Nallar, M.; Wong, H.-W., Hydroxyl Group Stabilization for Increased Yields of Low-Molecular-Weight Products in the Copyrolysis of Cellulose and Thermoplastics. *Ind. Eng. Chem. Eng.* **2019**, *58* (25), 10776-10784. DOI: 10.1021/acs.iecr.9b01177

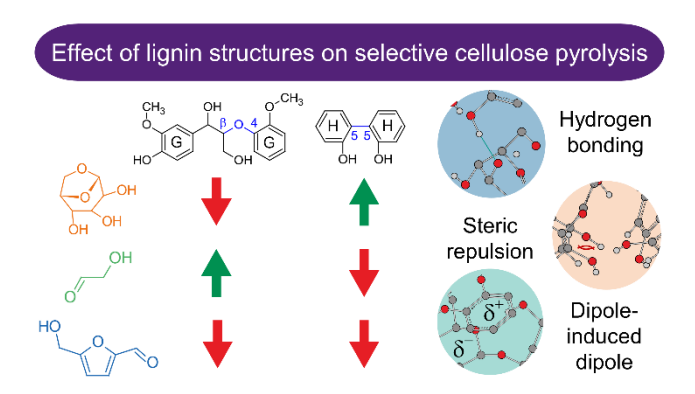
- 36. Nallar, M.; Wong, H.-W., Enhanced Levoglucosan Yields from the Copyrolysis of Cellulose and High-Density Polyethylene. *ACS Sustainable Chem. Eng.* **2019**, *7* (10), 9480-9488. DOI: 10.1021/acssuschemeng.9b00765
- 37. Westerhof, R. J. M.; Oudenhoven, S. R. G.; Marathe, P. S.; Engelen, M.; Garcia-Perez, M.; Wang, Z.; Kersten, S. R. A., The Interplay between Chemistry and Heat/Mass Transfer During the Fast Pyrolysis of Cellulose. *React. Chem. Eng.* 2016, 1 (5), 555-566. DOI: 10.1039/C6RE00100A
- 38. Patwardhan, P. R.; Dalluge, D. L.; Shanks, B. H.; Brown, R. C., Distinguishing Primary and Secondary Reactions of Cellulose Pyrolysis. *Bioresour. Technol.* **2011**, *102* (8), 5265-5269. DOI: https://doi.org/10.1016/j.biortech.2011.02.018
- 39. Pecha, M. B.; Montoya, J. I.; Chejne, F.; Garcia-Perez, M., Effect of a Vacuum on the Fast Pyrolysis of Cellulose: Nature of Secondary Reactions in a Liquid Intermediate. *Ind. Eng. Chem. Res.* **2017**, *56* (15), 4288-4301. DOI: 10.1021/acs.iecr.7b00476
- 40. Lin, Y.-C.; Cho, J.; Tompsett, G. A.; Westmoreland, P. R.; Huber, G. W., Kinetics and Mechanism of Cellulose Pyrolysis. *J. Phys. Chem. C* **2009**, *113* (46), 20097-20107. DOI: 10.1021/jp906702p
- 41. Hu, B.; Zhang, B.; Xie, W.-l.; Jiang, X.-y.; Liu, J.; Lu, Q., Recent Progress in Quantum Chemistry Modeling on the Pyrolysis Mechanisms of Lignocellulosic Biomass. *Energy Fuels* **2020**, *34* (9), 10384-10440. DOI: 10.1021/acs.energyfuels.0c01948
- 42. Mettler, M. S.; Paulsen, A. D.; Vlachos, D. G.; Dauenhauer, P. J., The Chain Length Effect in Pyrolysis: Bridging the Gap between Glucose and Cellulose. *Green Chem.* **2012**, *14* (5), 1284-1288. DOI: 10.1039/C2GC35184F
- 43. Degenstein, J. C.; Murria, P.; Easton, M.; Sheng, H.; Hurt, M.; Dow, A. R.; Gao, J.; Nash, J. J.; Agrawal, R.; Delgass, W. N.; Ribeiro, F. H.; Kenttämaa, H. I., Fast Pyrolysis of 13c-

Page 36 of 39

- Labeled Cellobioses: Gaining Insights into the Mechanisms of Fast Pyrolysis of Carbohydrates. *J. Org. Chem.* **2015**, *80* (3), 1909-1914. DOI: 10.1021/jo5025255
- 44. Lu, Q.; Hu, B.; Zhang, Z.-x.; Wu, Y.-t.; Cui, M.-s.; Liu, D.-j.; Dong, C.-q.; Yang, Y.-p., Mechanism of Cellulose Fast Pyrolysis: The Role of Characteristic Chain Ends and Dehydrated Units. *Combust. Flame* 2018, 198, 267-277. DOI: https://doi.org/10.1016/j.combustflame.2018.09.025
- 45. Paine, J. B.; Pithawalla, Y. B.; Naworal, J. D., Carbohydrate Pyrolysis Mechanisms from Isotopic Labeling: Part 2. The Pyrolysis of D-Glucose: General Disconnective Analysis and the Formation of C1 and C2 Carbonyl Compounds by Electrocyclic Fragmentation Mechanisms. *J. Anal. Appl. Pyrolysis* 2008, 82 (1), 10-41. DOI: https://doi.org/10.1016/j.jaap.2008.01.002
- 46. Mayes, H. B.; Nolte, M. W.; Beckham, G. T.; Shanks, B. H.; Broadbelt, L. J., The Alpha–Bet(a) of Glucose Pyrolysis: Computational and Experimental Investigations of 5-Hydroxymethylfurfural and Levoglucosan Formation Reveal Implications for Cellulose Pyrolysis. *ACS Sustainable Chem. Eng.* **2014**, *2* (6), 1461-1473. DOI: 10.1021/sc500113m
- 47. Zhang, J.; Choi, Y. S.; Yoo, C. G.; Kim, T. H.; Brown, R. C.; Shanks, B. H., Cellulose–Hemicellulose and Cellulose–Lignin Interactions During Fast Pyrolysis. *ACS Sustainable Chem. Eng.* **2015**, *3* (2), 293-301. DOI: 10.1021/sc500664h
- 48. Wang, S.; Guo, X.; Wang, K.; Luo, Z., Influence of the Interaction of Components on the Pyrolysis Behavior of Biomass. *J. Anal. Appl. Pyrolysis* **2011,** *91* (1), 183-189. DOI: https://doi.org/10.1016/j.jaap.2011.02.006
- 49. Sheng, Y.; Lam, S. S.; Wu, Y.; Ge, S.; Wu, J.; Cai, L.; Huang, Z.; Le, Q. V.; Sonne, C.; Xia, C., Enzymatic Conversion of Pretreated Lignocellulosic Biomass: A Review on Influence

- of Structural Changes of Lignin. *Bioresour. Technol.* **2021,** *324*, 124631. DOI: https://doi.org/10.1016/j.biortech.2020.124631
- 50. Yoo, C. G.; Meng, X.; Pu, Y.; Ragauskas, A. J., The Critical Role of Lignin in Lignocellulosic Biomass Conversion and Recent Pretreatment Strategies: A Comprehensive Review. *Bioresour. Technol.* **2020**, *301*, 122784. DOI: https://doi.org/10.1016/j.biortech.2020.122784
- 51. Zheng, A.; Chen, T.; Sun, J.; Jiang, L.; Wu, J.; Zhao, Z.; Huang, Z.; Zhao, K.; Wei, G.; He, F.; Li, H., Toward Fast Pyrolysis-Based Biorefinery: Selective Production of Platform Chemicals from Biomass by Organosolv Fractionation Coupled with Fast Pyrolysis. *ACS Sustainable Chem. Eng.* **2017**, *5* (8), 6507-6516. DOI: 10.1021/acssuschemeng.7b00622
- 52. Ullah, Z.; khan, M.; Raza Naqvi, S.; Farooq, W.; Yang, H.; Wang, S.; Vo, D.-V. N., A Comparative Study of Machine Learning Methods for Bio-Oil Yield Prediction a Genetic Algorithm-Based Features Selection. *Bioresour. Technol.* **2021**, *335*, 125292. DOI: https://doi.org/10.1016/j.biortech.2021.125292
- 53. Tang, Q.; Chen, Y.; Yang, H.; Liu, M.; Xiao, H.; Wang, S.; Chen, H.; Raza Naqvi, S., Machine Learning Prediction of Pyrolytic Gas Yield and Compositions with Feature Reduction Methods: Effects of Pyrolysis Conditions and Biomass Characteristics. *Bioresour. Technol.* **2021**, *339*, 125581. DOI: https://doi.org/10.1016/j.biortech.2021.125581

For Table of Contents Use Only



Synopsis

The multifaceted role of lignin on selective production of renewable bio-based chemicals from cellulose fast pyrolysis is demonstrated.